Terahertz optical properties of multilayer graphene: Experimental observation of strong dependence on stacking arrangements and misorientation angles

I-Tan Lin,[1] Jia-Ming Liu,[1,*] Kai-Yao Shi,[2] Pei-Shan Tseng,[2] Kuang-Hsiung Wu,[2] Chih-Wei Luo,[2] and Lain-Jong Li[3]

[1]*Electrical Engineering Department, University of California, Los Angeles, Los Angeles, California 90095, USA*

[2]*Department of Electrophysics, National Chiao-Tung University, Hsinchu, Taiwan*

[3]*Institute of Atomic and Molecular Sciences, Academia Sinica, Taipei 10617, Taiwan*

(Received 8 November 2012; published 27 December 2012)

The optical conductivity of monolayer and multilayer graphene in the terahertz spectral region is experimentally measured using terahertz time-domain spectroscopy. The stacking arrangement and the misorientation angle of each sample are determined by Raman spectroscopy. The chemical potential of each sample is measured using ultrafast midinfrared pump-probe spectroscopy to be 63 or 64 meV for all samples. The intraband scattering rate can be obtained by fitting the measured data with theoretical models. Other physical parameters, including carrier density, dc conductivity, and carrier mobility, of each sample can also be deduced from the theoretical fitting. The fitting results show the existence of misoriented or AA-stacked layers with an interaction energy of $\alpha_1 = 217$ meV in our multilayer samples. Here we show that the scattering rate strongly depends on the stacking arrangement of the sample. High scattering rates and high optical conductivity are associated with AA-stacked samples, while lower ones are associated with misoriented multilayer graphene. This implies that the THz optoelectronic properties of multilayer graphene can be tuned by purposefully misorienting layers or employing different stacking schemes.

DOI: 10.1103/PhysRevB.86.235446 PACS number(s): 78.67.Wj, 61.48.Gh, 72.80.Vp, 73.50.Mx

I. INTRODUCTION

Graphene has been a subject of intense interest in the research community since it was successfully isolated in 2004.[1] Due to its unique energy band structure, the frequency of the graphene plasmon and the band gap of the graphene nanoribbon are in the terahertz (THz) region.[2,3] Therefore, graphene is considered a promising material for THz optoelectronic devices, such as THz detectors and modulators.[4,5] The optical conductivity of graphene in the THz region also allows graphene to support nanoscale THz surface plasmonic applications.[6] To develop these graphene-based THz optoelectronic devices, it is of great importance to understand the optical properties of graphene in the THz spectral region. The optical conductivity of graphene in the THz spectral region has been measured by several groups using Fourier-transform infrared spectroscopy (FTIR)[7–9] or THz time-domain spectroscopy (THz-TDS).[10,11] However, there has been a lack of experimental studies on the optical conductivity in the THz spectral region of multilayer graphene with different stacking arrangements. In this paper, we report our measurements of the THz optical conductivity of graphene with different numbers of layers using THz-TDS. The obtained experimental data are fitted with models of different stacking schemes. Many key physical parameters, including the intraband carrier scattering rate, the carrier density, the dc conductivity, and the carrier mobility, are deduced from the theoretical fitting analysis of the experimental data. The stacking arrangement and the misorientation angle of each graphene sample are also determined with our best effort, and their implication for the physical parameters of the sample is clearly illustrated.

II. THEORECTICAL MODELS

In the THz spectral region, the optical conductivity of graphene is dominantly determined by the intraband carrier scattering.[12] Semiclassically, the intraband conductivity of monolayer graphene can be expressed as[12]

$$\sigma_{\text{mono}}(\omega) = \frac{e^2}{\pi\hbar^2}\frac{2kT}{\tau^{-1} - i\omega}\ln\left[2\cosh\left(\frac{\mu}{2kT}\right)\right], \qquad (1)$$

where e is the electric charge, $\hbar$ is Planck's constant, k is the Boltzmann constant, T is the temperature, τ is the relaxation time of carriers near the chemical potential, ω is the angular frequency of photons, and μ is the chemical potential (i.e., the Fermi level). Here and throughout the rest of this paper, we have assumed that the frequency dependence of τ is sufficiently weak so that it can be regarded as a constant. Our initial analysis shows that this is a good approximation in the THz spectral region of our interest in this paper. The frequency dependence of τ is an important subject to be further studied in our future research. Equation (1) can also describe the optical conductivity of misoriented (turbostratic) multilayer graphene, which is frequently observed in chemical vapor deposition (CVD) synthesis.[13,14] The energy dispersion of misoriented multilayer graphene is linear near the Dirac point, like that of monolayer graphene, but with a reduced Fermi velocity.[15] Because Eq. (1) is not a function of the Fermi velocity, it can also be used to calculate the optical conductivity per layer of misoriented multilayer graphene.

For AA- and AB-stacked multilayer graphene, however, the interlayer interaction greatly changes the band structure so that Eq. (1) is not accurate for these stacking schemes. AA-stacked N-layer graphene has a band structure consisting of N Dirac bands that are shifted in energy. The energy differences among these bands are $2\alpha_1\cos[r\pi/(N+1)]$,[16] where $r = 1,2,\ldots,N$ and α_1 is the interaction energy of vertically neighboring atoms. The interaction energy α_1 and the interlayer separation of AA-stacked graphene are not the same as those of AB-stacked graphene because the atomic arrangement of the system is fundamentally different for these

two stacking types. The interlayer separation is measured to be around 3.6 Å for the spacing between AA-stacked layers,[17] which leads to the value of $\alpha_1 = 217$ meV.[18,19] The optical conductivity per layer of AA-stacked multilayer graphene can be expressed as the average of the contribution from N different Dirac bands. Using Eq. (1), we obtain

$$\sigma_{\mathrm{AA}}(\omega) = \frac{e^2}{\pi\hbar^2 N}\frac{2kT}{\tau^{-1} - i\omega} \times \sum_{r=1,2..N} \ln\left(2\cosh\left\{\frac{\mu + 2\alpha_1\cos[r\pi/(N+1)]}{2kT}\right\}\right). \quad (2)$$

It is also possible that a multilayer graphene consists of misoriented layers as well as layers that are AA or AB stacked. For example, it has been suggested that for ABA′ graphene (an AB-stacked bilayer plus a misoriented monolayer), the Raman spectrum is the combination of the spectra from an AB-stacked bilayer and a misoriented monolayer,[20] and its band structure is a superposition of that of the AB-stacked bilayer and a linear dispersion band.[21] The superposition of band structures provides us with the convenience in calculating the optical conductivity of such a mixed system of different stacking schemes. In this case, the optical conductivity of ABA′ graphene is the sum of the optical conductivity of an AB-stacked bilayer and that of a misoriented monolayer. Here we generalize this conclusion to multilayer graphene comprising AA-stacked and misoriented layers as supported by the fitting results from our experimentally measured data described below. For example, from Eqs. (1) and (2), the optical conductivity of an AAA′ graphene trilayer, which comprises one AA-stacked bilayer and one misoriented monolayer, is $\sigma_{\mathrm{AAA'}} = 2 \times \sigma_{\mathrm{AA}}|_{N=2} + \sigma_{\mathrm{mono}}$. Hereafter, for the ease of reference, we shall call Eq. (1) the graphene or misoriented model, Eq. (2) the AA model, and any combination of them the mixed model.

III. EXPERIMENT

A. Sample preparation

Our graphene samples were synthesized by CVD on a copper substrate. By carefully controlling the airflow of a mixture of methane and hydrogen in a heated furnace, monolayer graphene was uniformly grown on a copper substrate. The samples were then spin coated with poly(methyl methacrylate) (PMMA). The PMMA/graphene can be detached from the copper substrate by etching the copper with an aqueous nitric acid solution. The detached PMMA/graphene was then transferred and deposited on the sapphire substrate by direct contact. The PMMA was dissolved subsequently, leaving monolayer graphene on our target substrate. PMMA residues on the sample were then eliminated by the annealing process. N-layer graphene samples were obtained by repeating the aforementioned process N times on the same sapphire substrate. For this work, we used five graphene samples on sapphire substrate with $N = 1,2,3,5$, and 7, respectively. The number of layers in each sample was confirmed by the quantized absorption level of each sample seen in the optical transmission measurement using broadband visible light, as shown in Fig. 1. The quantized absorption level can be tuned by varying the synthesis condition in the CVD process; for this reason, different values are observed by different groups.[22,23]

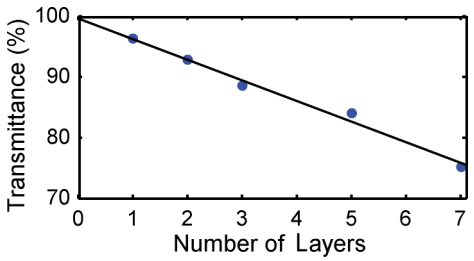

FIG. 1. (Color online) Transmittance (%) (measured at the wavelength of 600 nm) of samples with different numbers of graphene layers.

B. Raman spectroscopy

The Raman measurements were performed at room temperature under ambient conditions with a laser of 488-nm excitation wavelength and 5-mW power. As shown in Fig. 2, every one of the Raman G′-band spectra of our multilayer samples can be described by a single Lorentzian shape, which excludes the possibility of any of our samples being AB stacked.[24] Furthermore, except for the bilayer sample, the other multilayer samples ($N = 3$, 5, 7) all show a G′ blueshift with respect to that of the monolayer graphene (Table I). This indicates that the Fermi velocity is renormalized and some layers, if not all, are misoriented.[20,25] The G′-band intensity, shown in the inset of Fig. 2, is greatly influenced by the number of layers and the rotational angle of misorientation. It has been shown theoretically and experimentally that for misoriented bilayer graphene, the integrated intensity of the G′-band increases with inceasing rotational angle.[26,27] The integrated intensity can even be higher than twice that of monolayer graphene.[26] If this trend also applies to multilayer

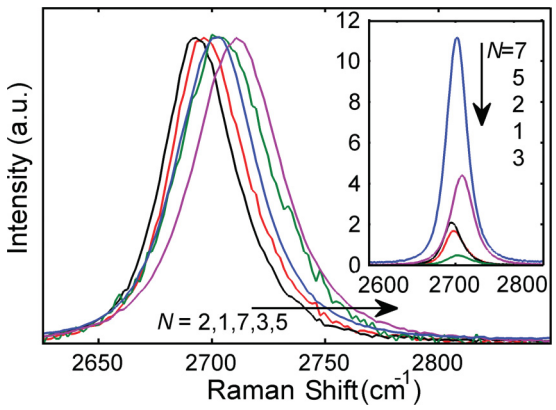

FIG. 2. (Color online) Raman G′-band spectra of monolayer ($N = 1$) and multilayer graphene with different numbers of layers ($N = 2$, 3, 5, 7). From left to right, as the arrow indicates, are curves for two-, one-, seven-, three- and five-layer graphene samples. The intensity is scaled to the same level to show the shifts of the curves. In the inset are the absolute Raman scattering intensities of the same data. Curves associated with different numbers of layers are indicated by the arrow. Corresponding curves are shown in the same color.

TABLE I. Raman G′-band shift and FWHM for graphene samples of different number of layers.

	Number of layers				
	1	2	3	5	7
G′ shift (cm^{-1})		–3	6	15	6
G′ FWHM (cm^{-1})	40	37	48	45	43

graphene with $N > 2$, the average rotational angle among layers in our trilayer graphene sample should be very small because of the ultralow G′-peak intensity and the large full width at half maximum (FWHM) of the G′-band spectrum observed for this sample (Table I), which are both signatures of a small rotational angle.[26] For our five- and seven-layer graphene samples, the peak intensity of the seven-layer sample is around seven times that of monolayer graphene while that of the five-layer sample is only about three times that of monolayer graphene. Therefore, we conlcude that the average rotational angle among layers in the seven-layer graphene sample is larger than that in the five-layer graphene sample. For our bilayer graphene sample, we believe that it has AA stacking because its Raman spectrum has no G′ blueshift and its G′-peak intensity is similar to that of the monolayer sample (Fig. 2 inset). The small redshift might be caused by the finite amount of charged impurity.[28]

C. Terahertz time-domain spectroscopy

To gain more physical details about our samples, THz-TDS is used to measure the THz optical conductivity. The THz-TDS experiments are briefly described in the following. The generation and detection of THz pulsed radiation using the free-space electro-optic sampling technique was set up on a mode-locked Ti:sapphire laser operating at 800-nm wavelength with 30-fs pulses at an 80-MHz repetition rate. The femtosecond-pulse laser beam was split into a pump beam and a probe beam. The THz pulses were generated by using the pump laser pulses to trigger a semi-insulating-InP photoconductive switch that consists of two parallel electrodes spaced 0.5 mm apart and biased with a dc voltage of 100 V. The generated THz-pulse beam was focused by a pair of off-axis parabolic mirrors onto a graphene sample at normal incidence with the incident THz electric field polarized parallel to the sample surface. The temporal electric-field-amplitude profile of an incident or transmitted THz pulse was sampled by scanning the delay between the pump and probe optical pulses. For this sampling measurement, the incident or transmitted THz pulse being measured was focused by another pair of off-axis parabolic mirrors on a 1-mm-thick (110)-ZnTe sensor crystal. The polarization of the optical probe beam changes when the ZnTe crystal was irradiated by the THz electric field. The THz-induced phase retardation of the optical probe beam was converted into an intensity modulation and detected by using balanced photodiodes. In order to avoid any undesirable effects from the humidity in the laboratory air, the THz-TDS system was placed in a Plexiglas box and was purged with dry nitrogen flow. The measured time-domain profile of the incident THz electric-field amplitude is shown by the gray curve (labeled E_i) in Fig. 3(a).

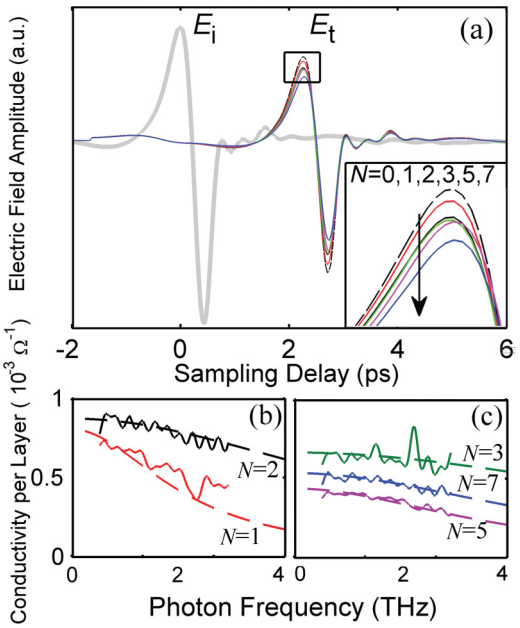

FIG. 3. (Color online) (a) Time-domain profiles of the incident electric-field amplitude (E_i) and the transmitted electric-field amplitudes (E_t) of THz pulses for the sapphire substrate and the graphene samples with different number of layers. E_i is obtained by measuring the transmitted signal through the air without the substrate in the optical path. The framed region of the transmitted profiles for E_t is enlarged and shown in the inset. Indicated by the arrow from top to bottom are the data for bare sapphire substrate ($N = 0$) and for graphene samples with $N = 1$, 2, 3, 5, 7 number of layers. (b), (c) Measured optical conductivity spectra (solid curves) and theoretical optical conductivity spectra (dashed curves) for (b) monolayer ($N = 1$) and bilayer graphene ($N = 2$), and (c) multilayer graphene ($N = 3$, 5, 7). Different models are used for fitting the experimental data of different samples (see text). The fitting values for the parameter τ^{-1} are presented in Table II(a).

All samples were measured at the room temperature of 294 K. For each sample before graphene was placed on the substrate, the time-domain profile of the transmitted electric-field amplitude of the THz pulse through the bare sapphire substrate was first measured as the background reference. After each sample with graphene on the sapphire substrate was made, the time-domain profile of the transmitted electric-field amplitude of the THz pulse through the sample was measured. These time-domain data are shown in Fig. 3(a). As can be seen, the transmitted signal is reduced as the number of layers increases. The spectra of the transmission coefficients in the frequency domain were obtained by taking the Fourier transform on the data in Fig. 3(a). The derived data are complex numbers, carrying both the phase and amplitude information. Using Maxwell's equations with appropriate boundary conditions, the ratio of the transmission coefficients t_{sam} (graphene sample on the sapphire substrate) to t_{sub} (bare sapphire substrate) in the frequency domain can be related to the optical conductivity of the graphene sample without the substrate as

$$\frac{t_{sam}(\omega)}{t_{sub}(\omega)} = \frac{1+n}{1+n+N\sigma(\omega)/c\varepsilon_0}, \tag{3}$$

TABLE II. Fitting results of scattering rate τ^{-1} for graphene samples of different number of layers. (a) Fitting results for τ^{-1} based on the assumption of possible AA stacking with experimentally measured values of chemical potential μ obtained by the pump-probe experiment. (b) Fitting results for μ and τ^{-1} based on the assumption that all samples are decoupled graphene layers.

		Number of layers				
		1	2	3	5	7
(a)	μ (meV)	64	64	64	63	63
	τ^{-1} (10^{12} s^{-1})	9.9	29.2	40.1	18	24.1
(b)	μ (meV)	91.4	190.9	248.1	70.3	114.9
	τ^{-1} (10^{12} s^{-1})	14.7	25.4	44.5	20.3	25.8

where $n = 3.07$ is the refractive index of the sapphire substrate, which was measured in our experiments and found to be consistent with literature;[29] c is the speed of light, ε_0 is the permittivity of free space, and $\sigma(\omega)$ is the measured optical conductivity per layer of the sample.

D. Ultrafast optical pump midinfrared probe experiment

We also experimentally obtained the chemical potential μ for each sample by using the ultrafast optical pump midinfrared probe technique.[30,31] Due to the redistribution around μ of the carriers excited by the optical pump pulse, the reflectivity of the sample increases ($\Delta R > 0$) for a probe photon energy higher than μ and decreases ($\Delta R < 0$) for a probe photon energy lower than μ. By finding the sign change of ΔR using different wavelengths of the midinfrared probe beam, the location of μ can be found. For all samples, μ was found to be 63 or 64 meV [Table II(a)]. The details of the measurement are beyond the scope of this paper.

IV. ANALYSIS AND DISCUSSIONS

With both μ and $\sigma(\omega)$ experimentally determined for each sample, we can now determine the scattering rate τ^{-1} and the stacking arrangement of each sample by fitting the real part of $\sigma(\omega)$ to the real part of our theoretical conductivity models using τ^{-1} as the fitting parameter. The fitting curves are shown in Figs. 3(b) and 3(c). The measured values of μ and the fitting values of τ^{-1} for these fitting curves are listed in Table II(a). We find that the monolayer and five-layer graphene samples fit well with the graphene/misoriented model. We have also tried fitting the data with the mixed model to see if there are AA-stacked layers in the five-layer sample. It is found that the theoretical optical conductivity is too high for the experimental data to be fitted with this model. For the bilayer and trilayer samples, the experimental data fit well with the AA model with an interaction energy of $\alpha_1 = 217$ meV, which is consistent with the theoretical value of α_1 reported in the literature.[18,19] Note that a different theoretical value of α_1 (361 meV) is also suggested in the literature,[32] which does not fit with our experimental data. This fitting result suggests that there are locally AA-stacked regions in our misoriented trilayer sample. The local existence of AA stacking is possible when layers are misoriented, as illustrated in Fig. 4(a). As suggested by its Raman spectrum in Fig. 2, our trilayer sample is misoriented with small rotational angles. Because the size of the local AA region in a unit cell increases rapidly with a rotational angle smaller than 5°,[15,33] we can potentially have an AA region that has a dimension comparable to the mean free path of carriers in the resultant supercell if the angle is sufficiently small. The Fermi velocity of AA-stacked trilayer graphene is about 8.37×10^5 m/s.[18] With a carrier lifetime of $\tau = 25$ fs that is obtained by fitting with the AA model, the mean free path is 20 nm, which is around one hundred lattice constants. Because the number of carbon atoms in a supercell can easily reach thousands,[33] it is possible that our conductivity data are the direct measurement of locally AA-stacked regions in the sample. For the seven-layer sample, $\sigma(\omega)$ fits well with a mixed model of five misoriented layers plus an AA-stacked bilayer. By comparison, the existence of AA-stacking coupling is difficult to tell from its Raman spectrum because it is overwhelmed by the Raman intensity contributed by the misoriented layers.

To further show the existence of AA stacking in our samples, we also fit the experimental data using Eq. (1) by assuming that all the samples have decoupled graphene layers, with both τ^{-1} and μ as fitting parameters. The fitting results are listed in Table II(b); they show a strong disagreement with the values of μ that were experimentally obtained by the pump-probe experiment. The large discrepancies in these fitting values of μ with its experimentally measured values cannot be explained by the inhomogeneity in the graphene layers or in the impurity density. Clearly, the assumption of decoupled graphene layers is not valid for all of our multilayer samples.

Other physical parameters can also be derived using the values of τ^{-1} and μ listed in Table II(a); the results are listed in Table III. With the Fermi velocity of monolayer $v_{\mathrm{F}}^{\mathrm{mono}} \cong 10^6$ m/s,[34] the mobility obtained for the monolayer graphene sample is very high, around 11 420 cm^2 V^{-1} s^{-1}. The mobility in a practical monolayer device might be much lower than this value as we have to consider the contact potential or ineffective gate coupling.[14,35] For AA-stacked bilayer and trilayer graphene samples, the carrier density can be calculated with known band overlapping and $v_{\mathrm{F}} \cong 8.37 \times 10^5$m/s.[18] The resultant mobilities for our bilayer and trilayer graphene samples as listed in Table III are below 1000 cm^2 V^{-1} s^{-1}, which are much lower than that of the monolayer sample. Also note that, as seen in Figs. 3(b) and 3(c), their optical

TABLE III. Derived physical parameters of graphene samples based on the parameters listed in Table II(a).

	Number of layers				
	1	2	3	5	7
Relaxation time τ (fs)	101	34.2	24.9	55.6	41.5
Carrier density (10^{12} cm^{-2}/layer)	0.44	5.58	7.22	0.48	1.91
dc conductivity (10^{-4} Ω^{-1}/layer)	8.04	8.82	6.33	4.25	5.25
Mobility (cm^2 V^{-1} s^{-1})	11420	987.9	547.9	5534	1718

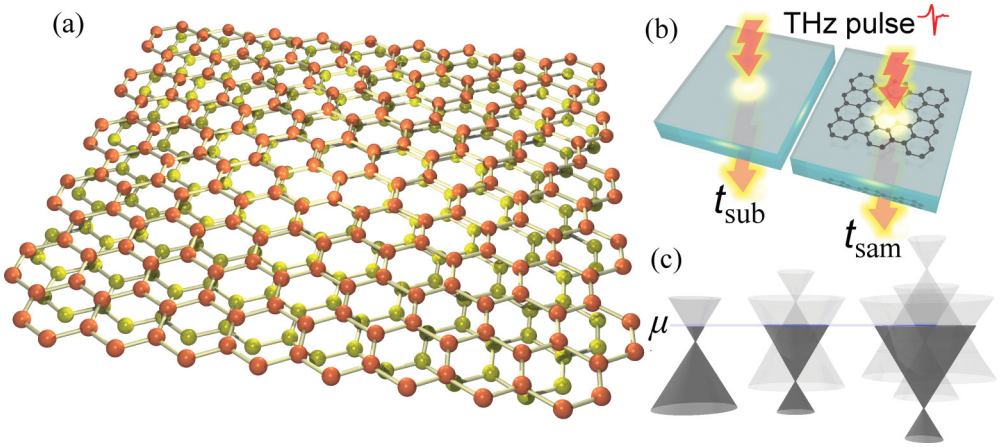

FIG. 4. (Color online) (a) Misoriented bilayer graphene with locally AA-stacked region illuminated by the incident THz pulse beam. (b) Schematically drawing of the transmission measurement without (t_{sub}) and with (t_{sam}) a graphene sample on a sapphire substrate. (c) From left to right: Filling of the lowest band by carriers in monolayer, AA-stacked bilayer, and AA-stacked trilayer graphene with the same chemical potential μ.

conductivities are relatively high among the samples due to the semimetal nature of AA stacking. For the five-layer sample, the average rotational angle is about 10° judging from its large blueshift of the G′ peak.[26] The corresponding Fermi velocity is $0.95v_F^{mono}$,[15] and the resultant carrier density and mobility are obtained and listed in Table III. For the seven-layer sample, its rotational angle is difficult to tell from its G′-peak shift because the observed shift corresponds to many possible angles.[26] However, because the peak intensity is almost seven times that of monolayer graphene, we can confidently assume that the rotational angle is sufficiently large that the Fermi velocity is the same as v_F^{mono}.[15] The obtained mobility is lower than that of the five-layer sample due to the existence of AA coupling in two of the layers in this seven-layer sample. From Table III we also notice that the scattering rate is relatively high for the bilayer and trilayer samples, which can be explained by the dependence of the scattering rate on the carrier density. For the same chemical potential, the carrier density is different in different subbands, as shown in Fig. 4(c) for the lowest conduction band. As can be seen, the carrier density is especially high in AA-stacked samples due to the large overlapping of bands. Because the scattering rate of short-range scatters is proportional to the square root of the carrier density ($\tau^{-1} \propto \sqrt{n}$),[35,36] our data indicate that short-range scatters are the dominant source of scattering in our bilayer and trilayer samples. Due to the AA-stacking coupling of two layers as suggested by the fitting result, our seven-layer sample also has a relatively high scattering rate. The sources of short-range scatters can be many, which cannot be identified from our experimental data.

To further confirm our fitting results, we calculated the refractive index $n(\omega) = \{[\varepsilon_\infty + i\sigma(\omega)/\omega d]/\varepsilon_0\}^{1/2}$, where d is the thickness per layer, $\sigma(\omega)$ is obtained from the experiment as in Eq. (3), and ε_∞, which is contributed by the interband transitions, is negligibly small compared to the other term for the THz frequency region.[37] We choose $d = 3.6$ Å (Ref. 17) for the bilayer and trilayer graphene samples (AA stacking), and 3.4 Å (Ref. 34) for the five- and seven-layer graphene samples (misoriented). The choice of 3.4 Å is an approximation as we are not able to accurately determine the rotational angles among the layers in the five-layer sample and in the seven-layer sample. Figure 5 shows, for each sample, the resultant refractive index that is deduced from the experimental data, plotted along with the theoretically calculated refractive index that is obtained using the appropriate model determined above for each sample. The values of the fitting parameter τ^{-1} listed in Table II(a) are used

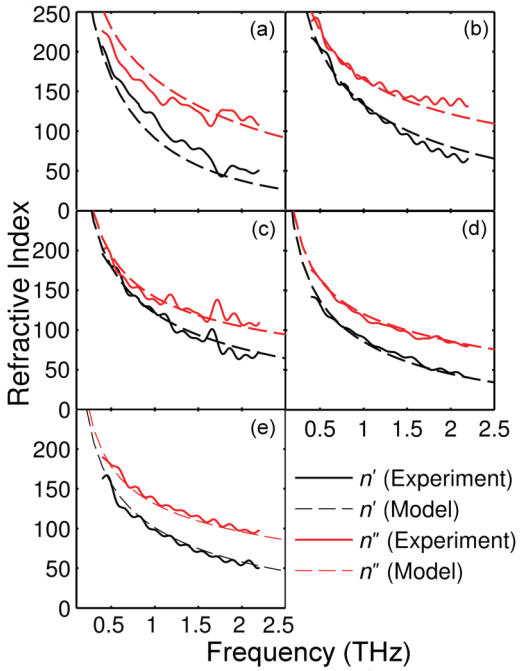

FIG. 5. (Color online) Measured refractive index (solid curves) and theoretically calculated refractive index (dashed curves) using a proper model for each sample (see text). n' and n'' are the real and imaginary parts of the refractive index, respectively. From (a) to (e) are the data for samples of one, two, three, five, and seven layers, respectively. Values of the fitting parameter τ^{-1} are listed in Table II(a).

for these theoretical calculations. As can be seen in Fig. 5, the experimental results can be fitted quite well by the theoretical models.

V. CONCLUSION

In summary, we have measured the THz optical conductivity of graphene samples that have different numbers of layers. The high conductivities and the Raman spectra of our bilayer and trilayer graphene samples suggest the existence of AA stacking of these samples. The experimental data can be fitted using the AA model with an interaction energy α_1 and an interlayer spacing that are both in very good agreement with those reported in the literature. Our five- and seven-layer graphene samples show the sign of rotational misorientation among layers as suggested in their Raman spectra and our fitting results. We also find that the scattering rate depends strongly on the stacking arrangement, with high scattering rates associated with AA-stacked samples and low scattering rates associated with misoriented multilayer samples. These studies and conclusions on graphene samples that appear in different rotational angles of misorientation and/or different stacking arrangements suggest that the transferring process in our CVD synthesis provides another degree of freedom in designing the electronic structure of multilayer graphene for desired electronic and optoelectronic characteristics.

ACKNOWLEDGMENTS

The coauthors at National Chiao-Tung University were financially sponsored by the National Science Council of Taiwan, R.O.C., under Grant No. NSC 98-2112-M-009-006-MY3 and by the Ministry of Education of Taiwan, R.O.C., under the 2011 MOE ATU program at NCTU.

*liu@ee.ucla.edu

[1] K. S. Novoselov, A. K. Geim, S. V. Morozov, D. Jiang, Y. Zhang, S. V. Dubonos, I. V. Grigorieva, and A. A. Firsov, Science **306**, 666 (2004).
[2] V. Barone, O. Hod, and G. E. Scuseria, Nano Lett. **6**, 2748 (2006).
[3] F. Rana, IEEE Trans. Nanotechnol. **7**, 91 (2008).
[4] F. Bonaccorso, Z. Sun, T. Hasan, and A. C. Ferrari, Nat. Photonics **4**, 611 (2010).
[5] B. Sensale-Rodriguez, T. Fang, R. Yan, M. M. Kelly, D. Jena, L. Liu, and H. Xing, Appl. Phys. Lett. **99**, 113104 (2011).
[6] A. Vakil and N. Engheta, Science **332**, 1291 (2011).
[7] H. Yan, F. Xia, W. Zhu, M. Freitag, C. Dimitrakopoulos, A. A. Bol, G. Tulevski, and P. Avouris, ACS Nano **5**, 9854 (2011).
[8] J. Horng, C.-F. Chen, B. Geng, C. Girit, Y. Zhang, Z. Hao, H. A. Bechtel, M. Martin, A. Zettl, M. F. Crommie, Y. R. Shen, and F. Wang, Phys. Rev. B **83**, 165113 (2011).
[9] H. Choi, F. Borondics, D. A. Siegel, S. Y. Zhou, M. C. Martin, A. Lanzara, and R. A. Kaindl, Appl. Phys. Lett. **94**, 172102 (2009).
[10] W. Liu, R. V. Aguilar, Y. Hao, R. S. Ruoff, and N. P. Armitage, J. Appl. Phys. **110**, 083510 (2011).
[11] J. L. Tomaino, A. D. Jameson, J. W. Kevek, M. J. Paul, A. M. van der Zande, R. A. Barton, P. L. McEuen, E. D. Minot, and Y.-S. Lee, Opt. Express **19**, 141 (2011).
[12] V. P. Gusynin, S. G. Sharapov, and J. P. Carbotte, New J. Phys. **11**, 095013 (2009).
[13] R. W. Havener, H. Zhuang, L. Brown, R. G. Hennig, and J. Park, Nano Lett. **12**, 3162 (2012).
[14] A. Reina, X. Jia, J. Ho, D. Nezich, H. Son, V. Bulovic, M. S. Dresselhaus, and J. Kong, Nano Lett. **9**, 30 (2008).
[15] G. Trambly de Laissardière, D. Mayou, and L. Magaud, Nano Lett. **10**, 804 (2010).
[16] H. Min and A. H. MacDonald, Prog. Theor. Phys. Suppl. **176**, 227 (2008).
[17] J.-K. Lee, S.-C. Lee, J.-P. Ahn, S.-C. Kim, J. I. B. Wilson, and P. John, J. Chem. Phys. **129**, 234709 (2008).
[18] I. Lobato and B. Partoens, Phys. Rev. B **83**, 165429 (2011).
[19] X. Yuehua, L. Xiaowei, and D. Jinming, Nanotechnology **21**, 065711 (2010).
[20] P. Poncharal, A. Ayari, T. Michel, and J. L. Sauvajol, Phys. Rev. B **78**, 113407 (2008).
[21] S. Latil, V. Meunier, and L. Henrard, Phys. Rev. B **76**, 201402 (2007).
[22] L. Gomez De Arco, Y. Zhang, C. W. Schlenker, K. Ryu, M. E. Thompson, and C. Zhou, ACS Nano **4**, 2865 (2010).
[23] X. Li, Y. Zhu, W. Cai, M. Borysiak, B. Han, D. Chen, R. D. Piner, L. Colombo, and R. S. Ruoff, Nano Lett. **9**, 4359 (2009).
[24] L. M. Malard, M. A. Pimenta, G. Dresselhaus, and M. S. Dresselhaus, Phys. Rep. **473**, 51 (2009).
[25] P. Poncharal, A. Ayari, T. Michel, and J. L. Sauvajol, Phys. Rev. B **79**, 195417 (2009).
[26] K. Kim, S. Coh, L. Z. Tan, W. Regan, J. M. Yuk, E. Chatterjee, M. F. Crommie, M. L. Cohen, S. G. Louie, and A. Zettl, Phys. Rev. Lett. **108**, 246103 (2012).
[27] Y. Hao, Y. Wang, L. Wang, Z. Ni, Z. Wang, R. Wang, C. K. Koo, Z. Shen, and J. T. L. Thong, Small **6**, 195 (2010).
[28] C. Casiraghi, S. Pisana, K. S. Novoselov, A. K. Geim, and A. C. Ferrari, Appl. Phys. Lett. **91**, 233108 (2007).
[29] D. Grischkowsky, S. Keiding, M. v. Exter, and C. Fattinger, J. Opt. Soc. Am. B **7**, 2006 (1990).
[30] R. A. Kaindl, M. Woerner, T. Elsaesser, D. C. Smith, J. F. Ryan, G. A. Farnan, M. P. McCurry, and D. G. Walmsley, Science **287**, 470 (2000).
[31] D. Sun, C. Divin, C. Berger, W. A. de Heer, P. N. First, and T. B. Norris, Phys. Rev. Lett. **104**, 136802 (2010).
[32] J. C. Charlier, J. P. Michenaud, and X. Gonze, Phys. Rev. B **46**, 4531 (1992).
[33] S. Shallcross, S. Sharma, E. Kandelaki, and O. A. Pankratov, Phys. Rev. B **81**, 165105 (2010).
[34] D. S. L. Abergel, V. Apalkov, J. Berashevich, K. Ziegler, and T. Chakraborty, Adv. Phys. **59**, 261 (2010).
[35] T. Stauber, N. M. R. Peres, and F. Guinea, Phys. Rev. B **76**, 205423 (2007).
[36] E. H. Hwang, S. Adam, and S. Das Sarma, Phys. Rev. Lett. **98**, 186806 (2007).
[37] E. A. Taft and H. R. Philipp, Phys. Rev. **138**, A197 (1965).